# Measuring the dynamics of second-order photon correlation functions inside a pulse with picosecond time resolution

**Assmann, Marc; Veit, Franziska; Tempel, Jean-Sebastian; Berstermann, Thorsten; Stolz, Heinrich; Poel, Mike van der; Hvam, Jørn Marcher; Bayer, Manfred**

*Published in:*
Optics Express

*Link to article, DOI:*
10.1364/OE.18.020229

*Publication date:*
2010

*Document Version*
Publisher's PDF, also known as Version of record

# Measuring the dynamics of second-order photon correlation functions inside a pulse with picosecond time resolution

**Marc Aßmann,[1,*] Franziska Veit,[1] Jean-Sebastian Tempel,[1] Thorsten Berstermann,[1] Heinrich Stolz,[2] Mike van der Poel,[3] Jørn M. Hvam,[3] and Manfred Bayer[1]**

[1]*Experimentelle Physik II, Technische Universität Dortmund, D-44221 Dortmund, Germany*
[2]*Fachbereich Physik, Universität Rostock, D-18501 Rostock, Germany*
[3]*DTU Fotonik, Technical University of Denmark, DK-2800 Kongens Lyngby, Denmark*
**marc.assmann@e2.physik.uni-dortmund.de*

**Abstract:** We present a detailed discussion of a recently demonstrated experimental technique capable of measuring the correlation function of a pulsed light source with picosecond time resolution. The measurement involves a streak camera in single photon counting mode, which is modified such that a signal at a fixed repetition rate, and well defined energy, can be monitored after each pulsed laser excitation. The technique provides further insight into the quantum optical properties of pulsed light emission from semiconductor nanostructures, and the dynamics inside a pulse, on the sub-nanosecond time scale.



**OCIS codes:** (030.5290) Photon statistics; (100.0118) Imaging ultrafast phenomena; (140.3948) Microcavity devices (250.5590) Quantum-well, -wire and -dot devices; (270.4180) Multiphoton processes; (320.7130) Ultrafast processes in condensed matter, including semiconductors.

## References and links

1. U. M. Titulaer, and R. J. Glauber, "Correlation functions for coherent fields," Phys. Rev. B **140**(3B), 676–682 (1965).
2. L. Mandel, "Sub-Poissonian photon statistics in resonance fluorescence," Opt. Lett. **4**(7), 205–207 (1979).
3. J. Wiersig, C. Gies, F. Jahnke, M. Aßmann, T. Berstermann, M. Bayer, C. Kistner, S. Reitzenstein, C. Schneider, S. Höfling, A. Forchel, C. Kruse, J. Kalden, and D. Hommel, "Direct observation of correlations between individual photon emission events of a microcavity laser," Nature **460**(7252), 245–249 (2009).
4. R. Loudon, "Non-classical effects in the statistical properties of light," Rep. Prog. Phys. **43**(7), 913–949 (1980).
5. H. Paul, "Photon antibunching," Rev. Mod. Phys. **54**(4), 1061–1102 (1982).
6. R. Hanbury Brown, and R. Q. Twiss, "Correlation between photons in two coherent beams of light," Nature **177**(4497), 27–29 (1956).
7. H. J. Kimble, M. Dagenais, and L. Mandel, "Photon antibunching in resonance fluorescence," Phys. Rev. Lett. **39**(11), 691–695 (1977).
8. S. Strauf, K. Hennessy, M. T. Rakher, Y. S. Choi, A. Badolato, L. C. Andreani, E. L. Hu, P. M. Petroff, and D. Bouwmeester, "Self-tuned quantum dot gain in photonic crystal lasers," Phys. Rev. Lett. **96**(12), 127404 (2006).
9. P. Michler, A. Kiraz, C. Becher, W. V. Schoenfeld, P. M. Petroff, L. Zhang, E. Hu, and A. Imamoglu, "A quantum dot single-photon turnstile device," Science **290**(5500), 2282–2285 (2000).
10. E. M. Purcell, "Spontaneous emission probabilities at radio frequencies," Phys. Rev. **69**, 681 (1946).
11. Z. Yuan, B. E. Kardynal, R. M. Stevenson, A. J. Shields, C. J. Lobo, K. Cooper, N. S. Beattie, D. A. Ritchie, and M. Pepper, "Electrically driven single-photon source," Science **295**(5552), 102–105 (2002).
12. M. Assmann, F. Veit, M. Bayer, M. van der Poel, and J. M. Hvam, "Higher-order photon bunching in a semiconductor microcavity," Science **325**(5938), 297–300 (2009).
13. F. Boitier, A. Godard, E. Rosencher, and C. Fabre, "Measuring photon bunching at ultrashort timescale by two-photon absorption in semiconductors," Nat. Phys. **5**(4), 267–270 (2009).
14. A. Hayat, A. Nevet, and M. Orenstein, "Ultrafast partial measurement of fourth-order coherence by HBT interferometry of upconversion-based autocorrelation," Opt. Lett. **35**(5), 793–795 (2010).
15. M. Aßmann, F. Veit, M. Bayer, S. Reitzenstein, S. Höfling, L. Worschech, and A. Forchel, "Ultrafast tracking of second-order photon correlations in the emission of quantum-dot microresonator lasers," Phys. Rev. B **81**(16), 165314 (2010).
16. G. Li, T. C. Zhang, Y. Li, and J. M. Wang, "Photon statistics of light fields based on single-photon-counting modules," Phys. Rev. A **71**(2), 023807 (2005).

#129614 - $15.00 USD Received 8 Jun 2010; revised 9 Jul 2010; accepted 16 Jul 2010; published 8 Sep 2010

## 1. Introduction

Only in few cases is the mean intensity sufficient for a complete characterization of a light field. More accurate descriptions are possible in terms of a hierarchy of correlation functions as defined by optical coherence theory [1]. While this concept has been used with great success in atom quantum optics [2], correlations have recently also attracted significant attention from solid-state physicists addressing the light generation from nanostructures [3]. Of particular interest is the normalized intensity correlation function of second order, defined as

$$g^{(2)}(t,\tau)=\frac{\left\langle \hat{a}^{\dagger}(t)\hat{a}^{\dagger}(t+\tau)\hat{a}(t)\hat{a}(t+\tau)\right\rangle}{\left\langle \hat{a}^{\dagger}(t)\hat{a}(t)\right\rangle\left\langle \hat{a}^{\dagger}(t+\tau)\hat{a}(t+\tau)\right\rangle}, \tag{1}$$

where $\hat{a}^{\dagger}$ and $\hat{a}$ are the photon creation and annihilation operators for the mode of interest evaluated at times $t$ and $t+\tau$, respectively. This function quantifies, how the detection of one photon from a light source influences the probability to detect another one. It usually decays to 1 on a timescale $\tau$ comparable to the coherence time of the light field [4]. The equal-time correlation function $g^{(2)}(t,0)$ already allows one to distinguish between thermal ($g^{(2)}(t,0)>1$), coherent ($g^{(2)}(t,0)=1$) and quantum ($g^{(2)}(t,0)<1$) light emission [5].

The typical experimental setup to measure this effect is the Hanbury Brown and Twiss (HBT) experiment [6], by which, for example, the quantum nature of the light emitted from single emitters has been demonstrated through the observation of antibunching [7]. Usually Si-avalanche photodiodes (APDs) were used as detectors in these experiments. The time resolution, which can be achieved by such detectors, is on the order of 500 ps (with high quantum efficiency) to 50 ps (with significantly reduced quantum efficiency). In order to check, whether the real (i.e. not masked by the finite experimental time resolution) intensity correlation function can be measured, the time resolution has to be compared to the coherence time of the light investigated [8]. The time resolution of APDs is often sufficient for light emission by atoms [9]. In semiconductors spontaneous emission occurs on a sub-nanosecond time scale with coherence times even shorter and often comparable to this time resolution. For semiconductor nanostructures in a microresonator, however, there may be a strong enhancement of the spontaneous decay rate due to the Purcell effect [10] so that the decay dynamics can no longer be resolved by such a setup due to the short coherence times.

It is often desirable to have access to the time dependence of $g^{(2)}$. Detection with APDs leads to averaging over the fluctuations of the correlation function that occur during the detection time, so that important information is blurred, for example concerning the transition from spontaneous to stimulated emission in microlaser structures, where the dynamics of interest take place on a picosecond time scale. Single-photon sources based on quantum dots are also operated by pulsed injection of electron-hole pairs [11]. The conversion to photons is stochastic, leading to a jitter of the emission. In order to obtain insight into this jitter, the correlation function has to be measured with a time resolution matching the light emission dynamics.

## 2. Experimental setup

Recently we presented results of $g^{(2)}$-measurements on a picosecond timescale [12]. We chose to use a modified streak camera as detector because it provides single-photon sensitivity together with a temporal resolution, which can be as short as 2 ps. Additionally, we also have the possibilities to measure higher order correlation functions directly at arbitrary delays and determine the dynamics of correlation functions inside pulses, which is not directly possible with other recently presented techniques [13,14]. Although we already gave a brief

#129614 - $15.00 USD Received 8 Jun 2010; revised 9 Jul 2010; accepted 16 Jul 2010; published 8 Sep 2010

explanation of our experimental setup in that publication, there is a need to discuss in more detail the general method, optimization schemes and data acquisition.

*2.1 General method of a streak camera*

In most common streak camera setups a spectrometer is used in front of the photocathode and the horizontal axis is imaged directly on the phosphorescent screen and used to achieve spectral resolution of the signal. The vertical axis provides the temporal resolution by applying a fast sinusoidal deflection voltage synchronously with the pulsed excitation laser. Usually, streak cameras are used to detect the integrated intensity of the signal of interest, which means that the signal after many pulsed excitations is accumulated at the same lateral position of the readout screen. This procedure only conserves information about the average intensity of the signal. All information about correlations is averaged out in integrated intensity measurements. In order to determine correlation functions at the single-photon level it is necessary to record single pictures. However, there is a good reason why streak cameras normally are used in integrated intensity mode. The frame rate of a CCD camera, which has a high enough quantum efficiency to detect the fluorescence of the phosphorescent screen, is on the order of 100 Hz at best. This means that only 100 pictures per second can be taken while the repetition rate of the excitation laser is much higher, 75.39 MHz in our case. Therefore only about 0.0001% of the signal is recorded, if single pictures are recorded instead of the integrated intensity.

*2.2 Optimization and customization*

In order to combine the recording of single pictures after each excitation with an acceptable ratio of recorded to total signal, we chose a different approach. In correlation experiments the intensity autocorrelation of one well-defined mode is normally of interest. Accordingly, there is no need to use a spectrometer and reserve the horizontal axis of the readout screen for spectral resolution. Instead we use an interference filter with 1-nm spectral width to single out the mode of interest. Now we use another set of deflection plates (oriented perpendicular to the normal ones) to which another, slower varying, sine voltage is applied, which causes a horizontal deflection of the electrons inside the streak camera. Due to the slow variation of the voltage, it is possible to record the emitted signals after several consecutive excitations next to each other at a different horizontal position on the same screen. In this manner, several dozen streaks can be recorded on a single picture instead of just one. Additionally, the electron amplification is switched off after the horizontal sweep and switched back on before the start of the next one to reduce noise accumulation. In general, a slower horizontal deflection allows for the simultaneous recording of a larger number of streaks. The minimal horizontal deflection speed is determined by the minimal distance between vertical streaks, which still makes it possible to distinguish two consecutive pulses positioned next to each other. Our streak camera allows for three different horizontal deflection times of 300, 600 or 1200 ns per horizontal screen width of 480 pixels. Our laser emits pulses every 13.2 ns. Under these circumstances the horizontal deflection time of 600 ns per screen allows us to record up to 45 streaks per single picture with a center to center distance of approximately 10 pixels between consecutive pulses and since even bad focusing usually does not lead to pulse widths larger than 8 pixels, they are still distinguishable. The horizontal deflection unit can be operated at a repetition rate of up to 15 kHz. To trigger it we use the same trigger signal as for the vertical deflection unit, but apply a frequency divider to start a horizontal sweep at every 6000th pulse only. Therefore a CCD camera with a frame rate, which matches the horizontal repetition rate, could in principle achieve duty cycles on the order of 1/110 for the 600 ns time window. Our CCD camera is currently limited to operation at 100 Hz and can therefore accumulate only 4500 pulse cycles per second. During the off-cycle the MCP is gated off. Faster CCD cameras or on-chip readout are promising candidates to overcome this readout speed limitation in the near future, allowing for much higher frame rates and more efficient measurements.

#129614 - $15.00 USD Received 8 Jun 2010; revised 9 Jul 2010; accepted 16 Jul 2010; published 8 Sep 2010

Such high frame rates pose a challenge for the phosphorescent screen. The most commonly chosen phosphor for streak camera screens is the P-43 phosphor, which has an afterglow decay time on the order of 1.5 ms, limiting readout rate to 600 Hz because the long lasting afterglow will cause also fluorescence from previous frames to be detected at the next frame, falsifying the information. Instead we use P-46 phosphor, which shows bi-exponential afterglow decay with the slower timescale in the range of tens of microseconds. The drawback of the P-46 phosphor is a reduced number of emitted photons per incident electron, by a factor of approximately 3 compared to the P-43 phosphor. This reduction is balanced by implementing a two-stage micro-channel plate, which allows us to increase the electron amplification from $10^3$ in the one-stage case to $10^5$ - $10^6$ in the two-stage case. Although the stronger amplification lowers the spatial resolution and therefore also the temporal resolution, our streak camera still showed a jitter-limited temporal resolution of 2 ps. Although not necessary for the currently used CCD operating at 100 Hz, usage of P-46 phosphor and a two-stage MCP ensure compatibility with improved future readout device designs.

Another common problem at high frame rates is the problem of data transfer. A single picture of 640 times 480 pixels with a data bit depth of 16 bits per pixel already has a size of roughly 0.6 MB. Therefore a frame rate of 10 kHz would already result in a data rate of 6 GB/s. In this regime, hard disk space, hard disk speed and the overhead for creating a new file for each picture are already limiting factors. This problem can be overcome by operating the camera in the so-called dynamic photon counting (DPC) mode. In this mode a whole sequence of pictures is saved into a single file instead of creating a new file for each picture in order to eliminate the overhead. Additionally, the amount of stored data is reduced drastically by storing only information about each detected photon. In each single picture most pixels will not contain any photons, so the amount of data is reduced significantly by storing the horizontal and vertical screen position of each photon and the frame number of that screen. By using the DPC mode the average file size occurring during our measurements has been reduced to approximately 1kB per 20 pictures at typical signal intensities.

*2.3 Data evaluation*

Now we present a detailed discussion on how to extract the intensity correlation function from the raw data. We use a data set of the emission from a planar semiconductor microcavity in the lasing regime using non-resonant optical pumping with 4 mW excitation power [12] as an example to visualize the technique. To calculate the intensity correlation function, one needs to know the number of photon pairs detected at times $t$ and $t+\tau$, respectively. This information can be extracted from the single pictures as follows: At first all photons in all pictures are sorted to streak bins with a width of one streak. Detected photons between two streaks are discarded. Now the desired temporal resolution $\Delta\tau$ is chosen by pixel binning within each streak bin, so that the streak bins are divided into time bins of a length corresponding to $\Delta\tau$.

It is therefore possible to analyze parts with different emission dynamics separately or to take only time bins with slowly varying mean photon count rates into account. Figure 1 shows an exemplary choice of variables for the binning process of the 4-mW excitation power data set used in [12]. The binned data set is analyzed with an algorithm that counts all – not just consecutive - photon pairs inside the streaks and sorts them according to the time of detection of the first photon and the time delay $\tau$. In the case of $\tau = 0$ this count is multiplied by 2 to account for the fact that the number of photon pairs counted in a bin containing *n* photons will be $n(n-1)/2$ while the definition of $g^{(2)}$ makes use of the photon number of the mode of interest before and after the detection of a photon, which gives a factor of $n(n-1)$. Dividing the number of pairs by the number of recorded single pictures already gives the photon pair counting rate for a certain combination of $t$ and $\tau$. Accordingly, a four-photon detection event, as depicted in the lower inset of Fig. 1, corresponds to twelve two-photon pairs.

#129614 - $15.00 USD Received 8 Jun 2010; revised 9 Jul 2010; accepted 16 Jul 2010; published 8 Sep 2010

To get the normalization, one also needs to know the expectation value of the number of photon pairs detected at the same times emitted by a light source with the same temporal profile, which emits photons statistically independent of each other. In the case of statistical independence the expectation value of photon pairs is given by the product of the mean photon count rates at times $t$ and $t+\tau$. This is exactly the information available in usual integrated intensity measurements. Accordingly we can directly get the mean photon count rates by integrating all the single pictures as shown in the upper panel of Fig. 1, thereby averaging out any effect of correlations. The normalized $g^{(2)}(t,\tau)$ is the measured photon pair count rate at times $t$ and $t+\tau$ as explained above divided by the product of the mean photon count rates at the same times.

Measurements of $g^{(2)}$ using a HBT setup are usually either done in CW mode, where there is no time dependence, or give a result, which is time averaged. We can time average our measured $g^{(2)}(t,\tau)$ to produce results, which are comparable to conventional HBT-measurements. This can be done by summing up all the photon pair count rates and dividing this number by the sum of the products of all photon count rates, which is equivalent to calculating the average of $g^{(2)}(t,\tau)$ weighted with respect to the photon numbers at times $t$ and $t+\tau$.

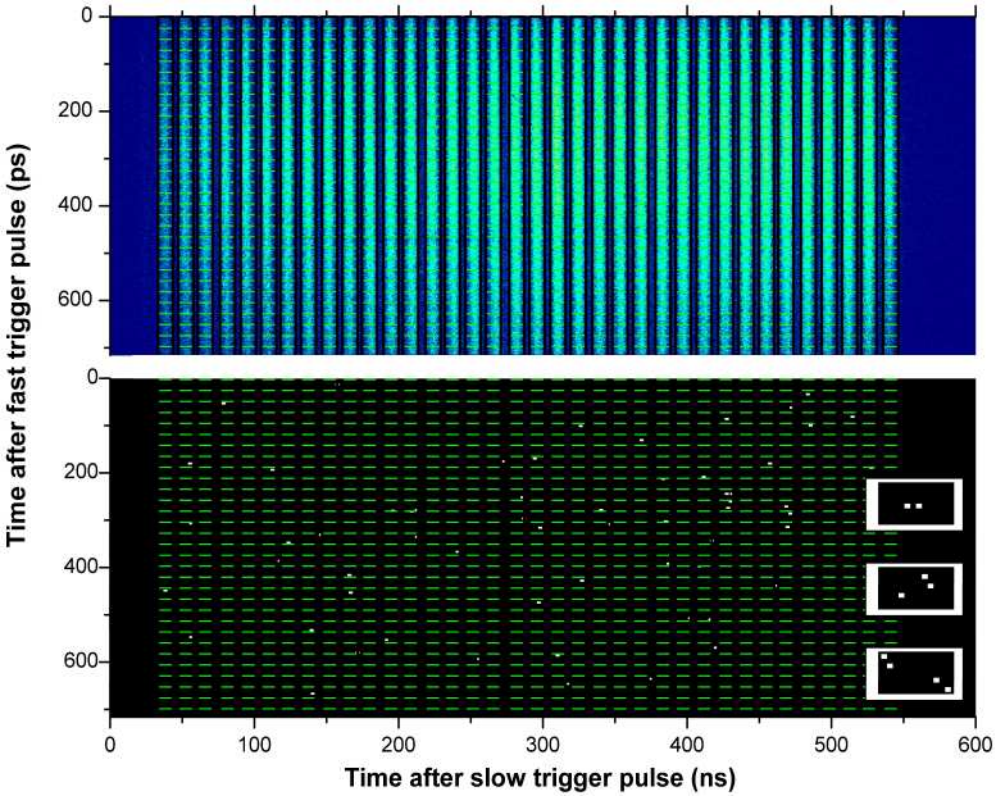


Fig. 1. Raw integrated (upper panel) and single-shot (lower panel) data acquired in intensity correlation measurements using a streak camera. The streak bins are shown with dark borders in the upper panel. The vertical distance between two green lines illustrates the pixel binning within the individual streak bins. Here the 700 ps streak bins are divided into 30 time bins. The insets show magnified time bins containing several photon combinations.

#129614 - $15.00 USD Received 8 Jun 2010; revised 9 Jul 2010; accepted 16 Jul 2010; published 8 Sep 2010

An exemplary data set based on the data of 60,000 single-shot measurements at a signal wavelength of approximately 800 nm is shown in Fig. 2. The horizontal axis is the time axis $t$. Black dots denote the square of the mean number of emitted photons at the corresponding times. It can be clearly seen that the intensity varies only very slowly with time. Red dots give the measured number of photon pairs at the corresponding times. As can be seen, the scatter of this data set is rather large. This is statistical noise, which could be further reduced by accumulating more data. Whether it is necessary to do so depends on the kind of information one wants to conclude from the data set above. It is possible to calculate $g^{(2)}(t,0)$ by dividing the number of measured photon pairs per time bin by the square of the mean photon number. This gives a time-resolved correlation function describing changes of the coherence during the pulse emission. If one was interested in such a measurement the statistical error of the data above is obviously too large to give significant results. However, in the data set above the intensity varies slowly and no significant changes of the coherence properties are expected at different times in the pulsed emission. Therefore it is possible to calculate a time averaged $g^{(2)}(0)$ by dividing the sum of the photon pair detection rates by the sum of the squared mean photon numbers. This averaging procedure reduces the statistical error significantly compared to that seen in Fig. 2 if there is no $t$-dependence of the correlation function. Calculating $g^{(2)}(0)$ in this manner for the data set shown in Fig. 2 for instance gives a result of 1.06 ± 0.03. It is possible to extend the analysis to higher-order correlation functions easily by calculating the count rates of three or more photons and dividing them by the product of the single photon count rates at

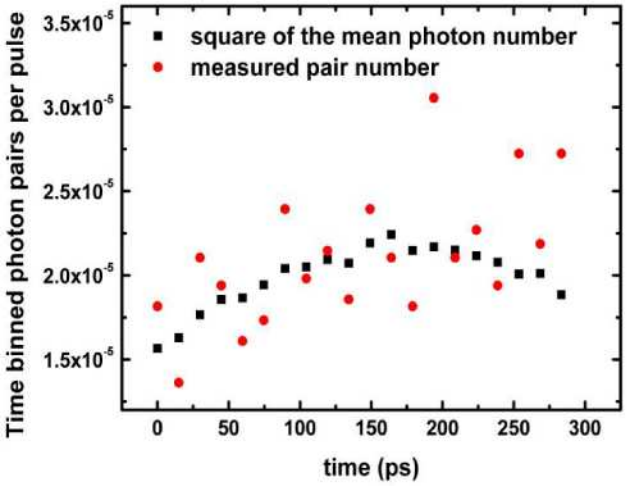


Fig. 2. Comparison of the number of detected photon pairs inside a time bin and the square of the mean photon number per time bin. The measured photon pair number has been multiplied by 2 and error-corrected as described in the text. Twenty time bins inside a 300 ps time window with slowly varying mean intensity have been chosen to exclude timing jitter effects. The data set used is the same, which was used for the 4mW excitation power data shown in Fig. 4 of reference [12].

the corresponding times. The third order correlation function is then given by:

$$g^{(3)}(t,\tau,\tau_2)=\frac{\left\langle \hat{a}^\dagger(t)\hat{a}^\dagger(t+\tau_1)\hat{a}^\dagger(t+\tau_1+\tau_2)\hat{a}(t)\hat{a}(t+\tau_1)\hat{a}(t+\tau_1+\tau_2)\right\rangle}{\left\langle \hat{a}^\dagger(t)\hat{a}(t)\right\rangle\left\langle \hat{a}^\dagger(t+\tau)\hat{a}(t+\tau)\right\rangle\left\langle \hat{a}^\dagger(t+\tau_1+\tau_2)\hat{a}(t+\tau_1+\tau_2)\right\rangle}. \quad (2)$$

However each additional order depends on one additional time delay compared to the lower order correlation function. The number of single pictures needed to achieve the same

#129614 - $15.00 USD Received 8 Jun 2010; revised 9 Jul 2010; accepted 16 Jul 2010; published 8 Sep 2010

relative error therefore increases with the order of the correlation function and so does the necessary computation times. Extracting $g^{(3)}(\tau_1 = \tau_2 = 0)$ from the same data set used above yields a result of 1.66±0.09.

*2.4 Error sources and error correction*

Our streak-camera method avoids some common error sources in typical HBT-type techniques with PD detection like afterpulsing, crosstalk and misalignment of the two detectors. It does, however, also introduce new error sources of which photon reconstruction is the most prominent one. Any detected photon will not fill exactly one pixel, but will have a size of several pixels. A built-in streak camera routine reconstructs the photon position on the screen by finding the center of gravity of the intensity measured at adjacent pixels. Local inhomogeneities of the streak camera screen can fool the photon reconstruction routine to consider one single photon as two. However, this problem can easily be detected by analysis of the distribution of pixel distances between two identified photons. Incorrect photon reconstruction will result in a distribution with very high pair count rates for pixel distances shorter than the radius $R$ of the photon size on the screen, which abruptly falls off step-like at distances, which are larger than $R$. To fix this problem, it is possible to introduce artificial dead pixels. If all photons detected within a distance of $R$ of another photon are disregarded, any erroneous photon counts due to reconstruction problems are eliminated. However in this way also real photon detections are disregarded. Effectively, the detector size for detecting another photon after the first one went down, which simply modifies the normalization by a factor of $wA'/A$ where $A$ is the size of a bin on the screen, $A'$ is the reduced size after introducing artificial dead pixels and $w$ is a weighting factor, which is needed, if the mean number of photon counts is not distributed equally along the width of a bin. If artificial dead pixels are used in measurements of higher-order correlation functions, it is necessary to consider the decreasing effective detector size inside a time bin accordingly after each photon detection. Fortunately the problem of erroneous photon reconstruction is usually only significant in analyzing a weak signal combined with a high electron gain and a fast horizontal blanking speed.

Sometimes it is also convenient to monitor the buildup of coherence over the duration of a pulse as given by $g^{(2)}(t,0)$. In these measurements the timing jitter of the signal can pose a problem for weak signals. Time bins with low photon pair count rates usually do not contribute strongly to a $g^{(2)}(\tau)$-measurement due to weighted averaging over all times *t*, but they need to be taken into account when measuring $g^{(2)}(t,0)$. In these bins usually no, or only few, photon pairs are detected. However, trigger timing jitter can cause a shift of the whole signal pulse on the screen, which in turn can cause a time bin with low photon pair count rates to be subject to a significantly increased intensity in some single picture, thereby causing a significant overestimation of $g^{(2)}(t,0)$. Fortunately, this overestimation is easily identified as $g^{(2)}(t,0)$ takes on very large values ranging from 4 up to 100 in this case, depending on the mean photon count rate of the time bin. If instead one is interested in determining the jitter, this effect can be used to determine its magnitude.

*2.5 Characterizing streak camera performance*

Exact knowledge of the streak camera temporal resolution, its timing jitter and the dark count rate can be crucial parameters in order to estimate whether it is sensible to perform streak-camera measurements of $g^{(2)}$. The easiest way to demonstrate the temporal resolution is a measurement of $g^{(2)}(\tau)$ for a thermal light source which has a coherence time on the order of

#129614 - $15.00 USD Received 8 Jun 2010; revised 9 Jul 2010; accepted 16 Jul 2010; published 8 Sep 2010

the temporal resolution. As these are generally hard to find, we instead measure $g^{(2)}(\tau)$ for a short laser pulse. In this regime the streak camera can be used in a manner similar to an autocorrelator and artificial bunching occurs on a very fast timescale. This artificial bunching can be explained by taking the effect of jitter on the normalization procedure into account. The time-integrated photon pair count rate is not sensitive to jitter. Although the peak position of the detected signal and the number of detected photon pairs in a certain time bin will vary slightly in each single picture taken, the pulse shape, the $\tau$-dependence of the photon pair count rate and the sum of all photon pairs detected in all time bins will not depend on jitter. However, the mean photon count rate used for the normalization procedure might be broadened by the jitter. Assuming the simple case of a Gaussian pulse shape $S(t)$ with amplitude of unity and standard deviation $W$ and Gaussian jitter $J(t)$ with standard deviation $J$, the broadened mean photon count rate will be the convolution of both, given by another Gaussian $S_j(t)$ with standard deviation $W_j = \sqrt{W^2 + J^2}$. The lowest possible magnitude of the jitter is determined by the temporal response of the photocathode. However, it can be increased by instabilities of the trigger signal or the laser used. Background noise is taken into account via a constant noise count rate $r_n$. The jitter-dependent $g_j^{(2)}(\tau)$ is then:

$$g_j^{(2)}(\tau) = \frac{\iint (S(\tau_2) + r_n)\left(S(\tau + \tau_2) + r_n\right) J(t - \tau_2)\, d\tau_2 dt}{\int (S_j(t) + r_n)(S_j(t + \tau) + r_n) dt}. \qquad (3)$$

This function consists of three parts as shown in Fig. 3. As the photon pair distribution is narrower than the squared mean photon count distribution, artificial bunching will occur around $\tau = 0$.

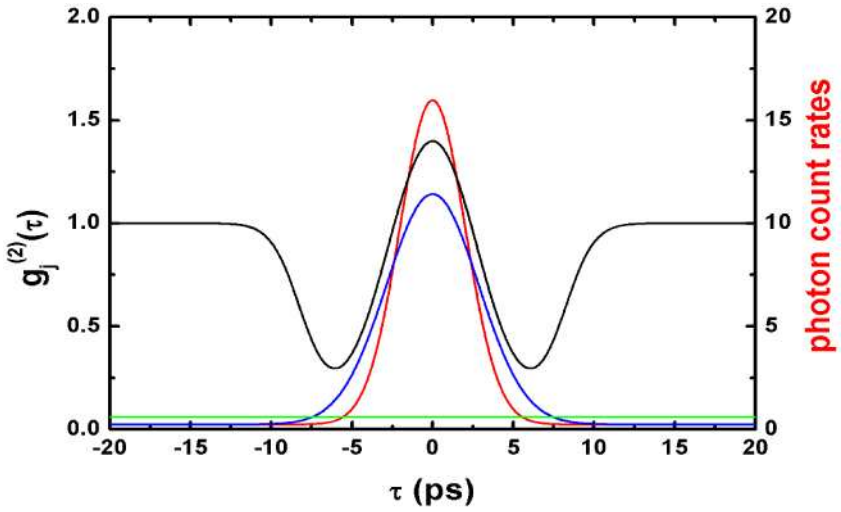


Fig. 3. Theoretical example for the jitter-affected shape of $g_j^{(2)}(\tau)$ shown as a black curve. The x-axis gives the delay $\tau$ for the black curve or the time $t$ for all other curves. Red and blue curves give the photon pair count rates and squared mean photon count rates, respectively. The green curve gives the constant background noise count rate. The resulting $g_j^{(2)}(\tau)$ shows values larger, smaller and equal to unity, depending on which of the count rates gives the dominant contribution at a given $\tau$.

#129614 - $15.00 USD Received 8 Jun 2010; revised 9 Jul 2010; accepted 16 Jul 2010; published 8 Sep 2010

As soon as the two distributions cross, $g_j^{(2)}(\tau)$ reaches values below unity. For large $\tau$ the cross-correlation between signal and background noise becomes dominant and $g_j^{(2)}(\tau)$ returns to unity. Based on $g_j^{(2)}(\tau)$ it is possible to characterize the streak camera performance for different settings of the MCP gain and the photon counting threshold by fitting the above equation to the experimental results. Some of these fits for different photon counting threshold and MCP gain settings are shown in Fig. 4 for a laser pulse with a standard deviation of 1.42 ps as evidenced by an autocorrelator. Here the smallest possible bin size of one pixel per bin, corresponding to a bin length of 283 fs, was used. At first sight a significant reduction of $g_j^{(2)}(\tau)$ near $\tau = 0$ is apparent. This is the effect of introducing artificial dead pixels as mentioned above. For $\tau$ which are larger than approximately 1 ps, this effect vanishes. For a MCP gain value of 40 (corresponding to a MCP voltage of 1.55 kV) a clear dependence of the shape of the intensity autocorrelation on the photon counting threshold can be seen. The data set for a low photon counting threshold (black squares) shows a deeper dip and larger artificial bunching compared to the data set obtained for a higher photon counting threshold (red dots). Fits to these two data sets are shown as black and red lines. The black line corresponds to values of $W$ =1.42 ps, $J$ =1.81 ps and $r_n$ =0.0015, while the red line corresponds to values of $W$ =1.42 ps, $J$ =1.38 ps and $r_n$ =0.0033. The low dark count rate shows that the low threshold value gives a very good signal-to-noise ratio, but also causes a large jitter and a slight underestimation of $g_j^{(2)}(\tau)$ for delays which are slightly larger than the delays covered by the dead pixels. This is an artifact caused by the photon reconstruction algorithm. For this special choice of settings, the photon size on the screen becomes rather large, but the intensity at many of the pixels is not too different from the threshold setting. In this case it becomes difficult to distinguish two different photons and they will be very often counted as a single one. This causes the slight underestimation at small $\tau$ and also explains the large jitter value because the center-of-gravity position of the intensity of these two photons on the screen is not too well defined. For the higher threshold value the jitter is significantly reduced and the underestimation of $g_j^{(2)}(\tau)$ has vanished, indicating that the photon reconstruction algorithm works better at these settings. The autocorrelation trace of the same signal at a higher gain setting of 42 (corresponding to 1.587 kV) is shown in the right panel. Here the data sets for low and high threshold settings are both fitted well using the same parameters applied to the high threshold data set in the left panel. The data set for the high threshold value shows good agreement, while the data set for the low threshold still shows some underestimation of the values for small $\tau$. This shows that still two photons are sometimes counted as one, but the higher gain causes more pixels to contain intensity values above the threshold setting, allowing for an easier estimation of the center-of-gravity by the photon reconstruction algorithm. Taking single photon sources into account, one might be interested in whether a streak-camera approach allows for unperturbed measurements of photon statistics in terms of quantum efficiency and dark count. There is no general answer to this question as both can depend on signal wavelength and the experimental conditions. Our streak camera is equipped with a S-20 photocathode with a radiant sensitivity above 10 mA/W in the visible wavelength range. The P-46 phosphor emits approximately 90 photons per incident electron. The exact efficiency of the total camera therefore depends crucially on the wavelength and gain used, but will usually not exceed 10%.

#129614 - $15.00 USD Received 8 Jun 2010; revised 9 Jul 2010; accepted 16 Jul 2010; published 8 Sep 2010

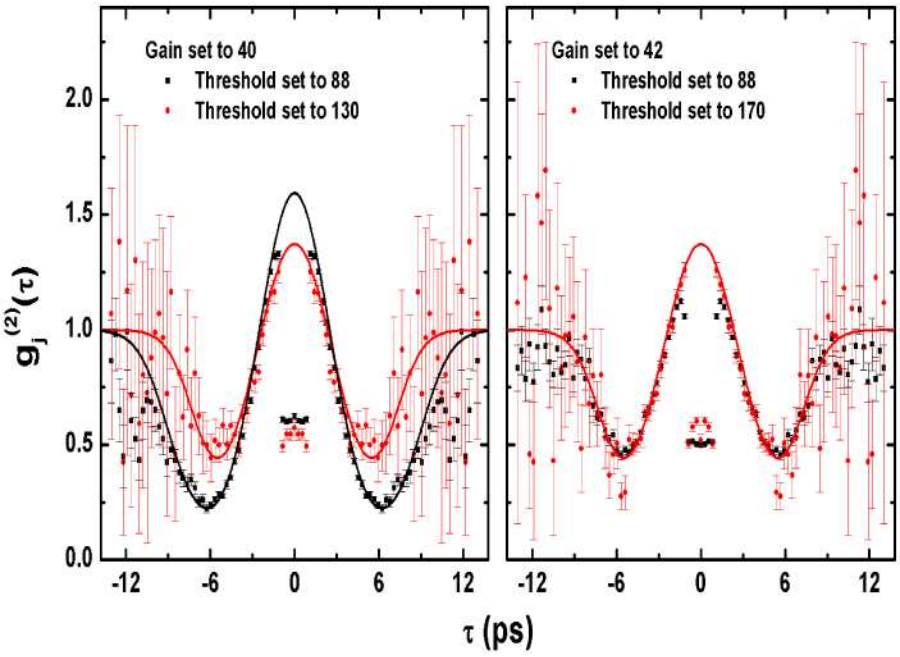


Fig. 4. Jitter-induced autocorrelation trace of a laser pulse at a wavelength of 768 nm with FWHM of 3.34 ps (corresponding to a standard deviation of 1.42 ps) for gain settings of 40 (left panel) and 42 (right panel). Experimental results for low and high threshold settings are shown as black and red dots, respectively. Solid lines represent fits to $g_j^{(2)}(\tau)$. The red lines correspond to fits for $J$ = 1.38 ps, $W$ = 1.42 ps and $r_n$ = 0.0033. The black line corresponds to a fit for $J$ = 1.81 ps, $W$ = 1.42 ps and $r_n$ = 0.0015.

However, the significant shape of $g_j^{(2)}(\tau)$ for a laser pulse with known wavelength and FWHM allows estimating the dark count rate under well-defined experimental conditions and is therefore an easily accessible indicator of the usefulness of the streak camera approach for single photon sources in a certain wavelength regime.

The increased bunching seen for small $\tau$ will also pose a problem when trying to address the intensity correlation of short signals. Experimentally the most relevant quantities are the time-integrated equal time correlation functions of second and third order. If the influence of dark noise is small, the measured value $g_j^{(2)}(0)$ can easily be corrected for pulses with Gaussian or similar shape. In second and third order the real and measured correlation functions are connected by:

$$g_j^{(2)}(0) = g^{(2)}(0)\sqrt{1+\frac{J^2}{W^2}},$$

$$g_j^{(3)}(0,0) = g^{(3)}(0,0)(1+\frac{J^2}{W^2}). \qquad (5)$$

As shown in Fig. 5, the deviations become significant if the jitter width is on the order of 20% of the signal width or larger.

#129614 - $15.00 USD Received 8 Jun 2010; revised 9 Jul 2010; accepted 16 Jul 2010; published 8 Sep 2010

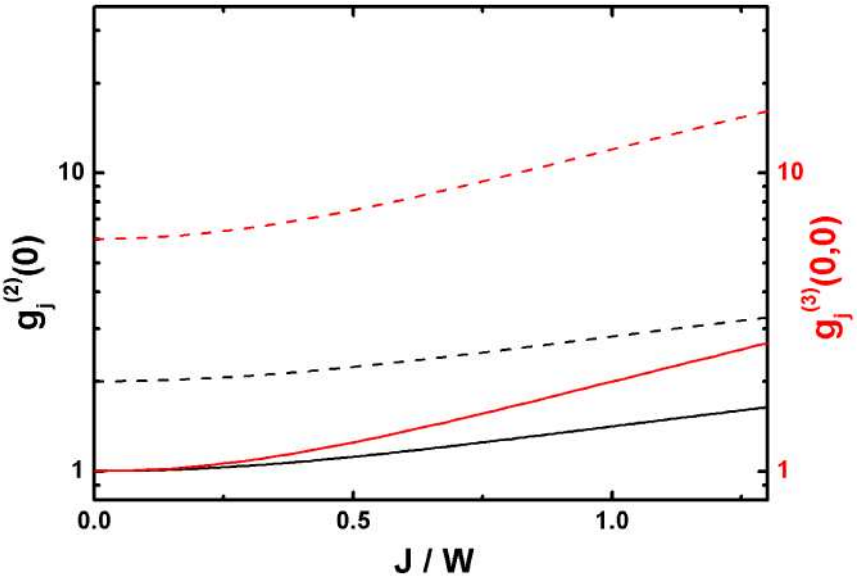


Fig. 5. Calculated second-order (black lines) and third-order (red lines) jitter-influenced correlation functions on a logarithmic scale. Solid and dashed lines represent coherent and thermal light, respectively.

Using the streak camera technique it is also possible to measure $g_j^{(2)}(\mathrm{t},0)$ as demonstrated in [15]. This quantity also shows a strong jitter-dependence for short pulses. For Gaussian pulse shapes, an analytical solution is given by:

$$g_j^{(2)}(t,0)=\frac{g^{(2)}(t,0)}{\left(r_n+\frac{e^{-\frac{t^2}{2W_j^2}}}{\sqrt{2\pi}W_j}\right)^2}\left(r_n^2+\frac{r_n e^{-\frac{t^2}{2W_j^2}}}{\sqrt{2\pi}W_j}+\frac{1}{2}\left(\frac{e^{-\frac{t^2}{B^2}}}{\pi WB}+\frac{r_n\sqrt{\frac{2}{\pi}}e^{-\frac{t^2}{2W_j^2}}}{W_j}\right)\right). \qquad (6)$$

Results for some pulse widths are shown in Fig. 6. An enhanced bunching at the pulse peak position ($t$=0) is clearly seen. This increase in $g_j^{(2)}(\mathrm{t},0)$ tends to become even larger in a narrow range around the origin, which tends to broaden with increased $W$. The reason for this effect lies in the relevant influence of large jitter values on pair detections at pulse positions with small mean intensity. Jitter causes the pulse peak to fall on a slightly different vertical position on the phosphorescent screen in each single picture taken. For pulses with slowly varying temporal shape, the change in the single picture intensity at one screen position due to this jitter-caused pulse position shifts will be small compared to the fluctuations around the mean intensity caused by intrinsic fluctuations due to the photon statistics. If $W$ and $J$ are comparable, the fluctuations in the single picture intensity at one screen position are not necessarily predominantly caused by the underlying photon statistics. The additional fluctuations caused by jitter-induced pulse position shifts affect regions with low mean intensity more strongly because the relative weight of a single screen with many photon pair counts at a screen position of low mean intensity will be larger than the relative weight of a single screen with few photon pair counts at a position of high mean intensity. For regions with low mean intensity this corresponds to large shot-by-shot photon number fluctuations and causes the significant overshoot seen in $g_j^{(2)}(\mathrm{t},0)$ away from the origin. In regions with

#129614 - $15.00 USD Received 8 Jun 2010; revised 9 Jul 2010; accepted 16 Jul 2010; published 8 Sep 2010

even lower mean intensity the contribution of noise becomes the dominant source of the mean intensity and even the rate of large jitter events shifting intensity to these positions vanishes. In this region $g_j^{(2)}(\mathrm{t},0)$ decays back to the uncorrelated value of unity. This explains also the broadening of the overshoot region as the onset of the noise-dominated pulse region shifts to larger times with increased $W$. However, in real situations also non-Gaussian jitter might occur due to instability of the laser or other external influences on the trigger timing accuracy. If those are present, too, they can shift some intensity to the noise-dominated region, causing rather high values of $g_j^{(2)}(\mathrm{t},0)$ there.

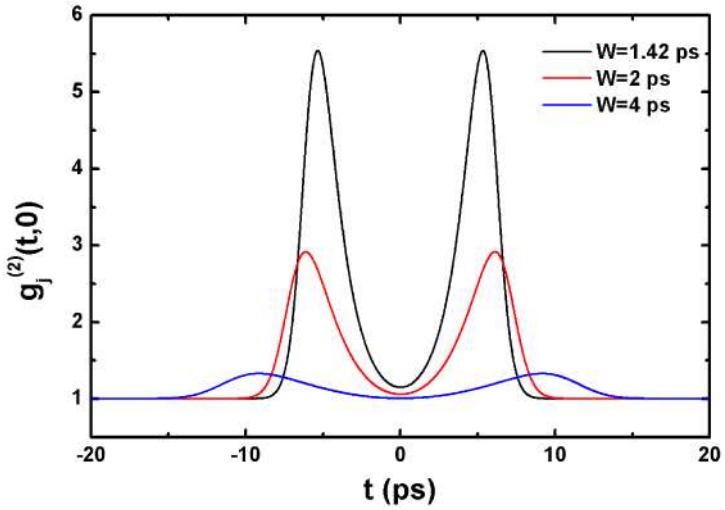


Fig. 6. Calculated second order jitter-influenced, time-resolved correlation functions of a coherent pulse for fixed values of $J$ =1.38 ps and $r_n$ =0.0033. Black, red and blue lines represent values of $W$ =1.42, 2 and 4 ps, respectively.

As a final figure of merit, it is worthwhile to discuss the influence of the detector time resolution on the measured $g^{(2)}$. As the streak-camera approach allows one to choose the effective temporal resolution $t_{IRF}$ in terms of an effective instrument response function by varying the size of time bins after data acquisition, it is not always necessary to use the best possible resolution of approximately 2 ps. The best choice will be a tradeoff between choosing a temporal resolution which is not distorting the results and having enough detections in each time bin to get a small statistical error. The temporal resolution is indeed the most important factor to consider in time-integrated measurements of $g^{(2)}$. The other prominent source for deviations between the real and the measured $g^{(2)}$ for thermal light using photodiodes in HBT-geometry - the inability of photodiodes to distinguish between single-photon and multi-photon arrivals inside one pulse cycle [16] - is not present using a streak-camera approach. Assuming a thermal signal for which a dependence of second order coherence on first order coherence $g^{(1)}(\tau)$ given by the Siegert relation

$$g^{(2)}(\tau) = 1 + |g^{(1)}(\tau)|^2 \tag{7}$$

is valid, $g_{IRF}^{(2)}(\tau)$ will be the convolution of the real signal and the instrument response function and $g_{IRF}^{(2)}(0)$ will depend strongly on the ratio between $t_{IRF}$ and the signal coherence

#129614 - $15.00 USD Received 8 Jun 2010; revised 9 Jul 2010; accepted 16 Jul 2010; published 8 Sep 2010

time $\tau_c$. This dependence is shown in Fig. 7. The deviations are small as long as $t_{IRF}$ does not exceed approximately 30% of $\tau_c$. Beyond this point the measured value will differ strongly from the real value of 2, showing already a difference of almost 20% in the deviation from the uncorrelated case, when $t_{IRF}$ equals $\tau_c$. Taking the best temporal resolution of the streak camera, it is be possible to measure coherence properties of signals with coherence times as short as 4 ps without significant deviations using the streak camera approach.

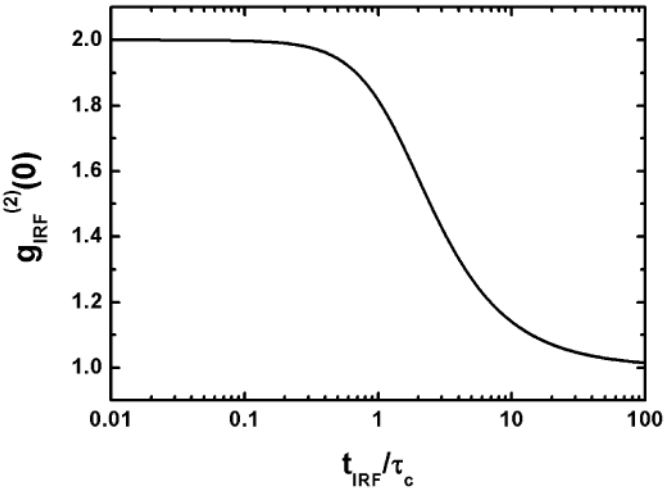


Fig. 7. Calculated correlation function $g_{IRF}^{(2)}(0)$ as a function of the ratio of the detector temporal resolution and the signal coherence time for thermal light with $g^{(2)}(0) = 2.$

## 3. Conclusion

In conclusion, we have demonstrated a single detector scheme using a streak camera suitable for a detailed mapping of the intensity correlation function of pulsed signals on the single-photon level. A temporal resolution of down to 2 ps can be achieved combined with the possibility to calculate averaged or un-averaged values for $g^{(2)}$ from the same set of data. The scheme can be generalized to higher-order correlation functions. We have presented a method to estimate the usefulness of the streak-camera approach under varying experimental conditions. Our scheme is useful for characterization of different classes of emitters ranging from thermal sources and lasers to non-classical light sources.


## Acknowledgements

This work was supported by the Deutsche Forschungsgemeinschaft research group “Quantum optics in semiconductor nanostructures” and the DFG research under grant No. DFG 1549/19-1.


#129614 - $15.00 USD Received 8 Jun 2010; revised 9 Jul 2010; accepted 16 Jul 2010; published 8 Sep 2010